HHS Public Access

Author manuscript

Hepatology. Author manuscript; available in PMC 2025 February 01.

Published in final edited form as:

Hepatology. 2024 February 01; 79(2): 409–424. doi:10.1097/HEP.0000000000000537.

Myeloid-specific ablation of Basp1 ameliorates diet-induced NASH in mice by attenuating pro-inflammatory signaling

Ziyi Meng[1], **Linkang Zhou**[1], **Sungki Hong**[2], **Xiaoxue Qiu**[1], **Zhimin Chen**[1], **Tongyu Liu**[1], **Ken Inoki**[2], **Jiandie D. Lin, Ph.D.**[1,*]

[1]Life Sciences Institute and Department of Cell & Developmental Biology, University of Michigan Medical Center, Ann Arbor, MI 48109

[2]Life Sciences Institute and Department of Molecular & Integrative Physiology, University of Michigan Medical Center, Ann Arbor, MI 48109

Abstract

Nonalcoholic steatohepatitis (NASH) represents a severe stage of fatty liver disease characterized by hepatocyte injury, inflammation, and liver fibrosis. Myeloid-derived innate immune cells, such as macrophages and dendritic cells, play an important role in host defense and disease pathogenesis. Despite this, the nature of transcriptomic reprogramming of myeloid cells in NASH liver and its contribution to disease progression remain incompletely defined. In this study, we performed bulk and single-cell RNA sequencing analysis to delineate the landscape of macrophage and dendritic cell transcriptomes in healthy and NASH liver. Our analysis uncovered cell type-specific patterns of transcriptomic reprogramming upon diet-induced NASH. We identified Brain abundant membrane attached signal protein 1 (Basp1) as a myeloid-enriched gene that is markedly induced in mouse and human NASH liver. Myeloid-specific inactivation of Basp1 attenuates the severity of diet-induced NASH pathologies as shown by reduced hepatocyte injury and liver fibrosis in mice. Mechanistically, cultured macrophages lacking Basp1 exhibited diminished response to pro-inflammatory stimuli, impaired NLRP3 inflammasome activation, and reduced cytokine secretion. Together, these findings uncover Basp1 as a critical regulator of myeloid inflammatory signaling that underlies NASH pathogenesis.

Graphical Abstract

*Corresponding author: Jiandie Lin, Ph.D., 5437 Life Sciences Institute, University of Michigan, 210 Washtenaw Avenue, Ann Arbor, MI 48109, jdlin@umich.edu, Office: (734) 615-3512.

Author contributions

J.D.L., and Z.M. conceived the project and designed research. Z.M., L.Z., S.H., X.Q., and Z.C. performed the experiments and analyzed the data. Z.M., X.Q., and T.L. performed sequencing data analyses. S.H., and K.I. generated Basp1 floxed mouse strain. J.D.L. and Z.M. prepared the manuscript.

Supplementary information

Two supplementary figure (Figure S1–S2) and five supplementary tables (Table S1–S5) are available online.

Competing interests

The authors declare no competing interests.

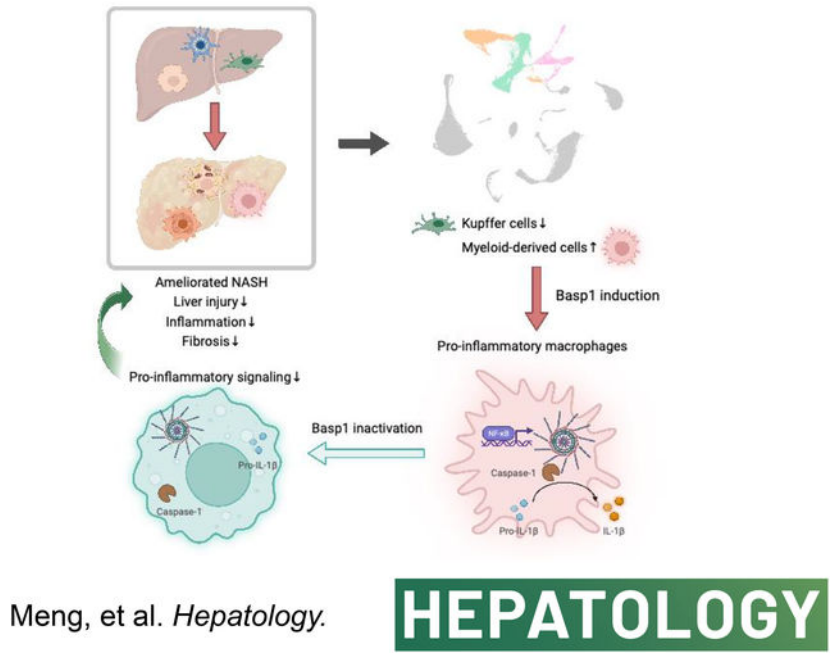

Meng, et al. *Hepatology.* HEPATOLOGY

Introduction

Nonalcoholic fatty liver disease (NAFLD) is characterized by aberrant fat accumulation in the liver and represents hepatic manifestation of the metabolic syndrome (1). NAFLD comprises a spectrum of metabolic liver disorders, ranging from simple steatosis to nonalcoholic steatohepatitis (NASH) (2–4). Patients with NASH exhibit varying degrees of liver injury, inflammation, and liver fibrosis, and are predisposed to end-stage liver diseases, such as cirrhosis and hepatocellular carcinoma. Several pathogenic factors have been identified that contribute to fat accumulation in the liver, including insulin resistance, adipose tissue dysfunction, and excess *de novo* lipogenesis. However, the pathophysiological mechanisms that govern the transition from simple steatosis to NASH remain incompletely defined.

Progressive remodeling of liver microenvironment is an integral aspect of NASH pathogenesis and encompasses transcriptomic and functional alterations of diverse cell types in the liver (5). Recent single-cell RNA sequencing (sc-RNAseq) studies have provided new insights into the landscape of liver cell heterogeneity and reprogramming in healthy and NASH liver, including hepatocytes and nonparenchymal cells (NPCs) (6–9). Beyond the dysregulations of metabolic gene expression, ectopic activation of signaling pathways unique to the disease state, such as TrkB-T1 and EphB2, has been implicated in exacerbating hepatocyte injury and NASH progression (10, 11). The liver sinusoidal endothelial cells adopt capillarization features in NASH that are marked by a loss of fenestrations and formation of a continuous basal membrane (12). In parallel, quiescent hepatic stellate cells (HSCs) undergo a phenotypic shift toward activated myofibroblasts, which drive increased synthesis and deposition of collagen matrix and liver fibrosis (6, 8, 13).

The innate immune cells play an important role in setting the balance between pro-inflammatory and anti-inflammatory signaling in NASH liver (14, 15). Notably, pro-inflammatory signaling via activation of the NLRP3 inflammasome promotes NASH progression, whereas pharmacological and genetic inactivation of NLRP3 protects mice from diet-induced NASH (16–19). We and others recently described a novel population of NASH-associated macrophages (NAMs) that express high levels of Trem2 (7, 9, 20), a gene associated with microglial function and the risk for Alzheimer's Disease. Hepatic NAMs originate from the hematopoietic compartment during NASH and NASH-associated liver cancer (20, 21). Further, lineage-tracing studies have established that NASH leads to a depletion of liver resident macrophages, which are replaced by monocyte-derived macrophages displaying molecular characteristics of Kupffer cells (KCs) (20). As such, it is likely that Trem2+ KCs may represent macrophages of bone marrow origin that acquire molecular signatures of KCs within the NASH liver microenvironment. While the exact role of NASH-associated macrophages in disease progression remains to be fully established, recent studies demonstrated that Trem2 ablation exacerbates hepatic inflammation and diet-induced NASH pathologies (22, 23). Trem2+ macrophages are capable of efferocytosis of dead hepatocytes suffered from lipotoxicity, thereby attenuating low-grade inflammation (23). These results suggest that NAMs may serve a protective role during disease progression.

Brain abundant membrane attached signal protein 1 (BASP1) is a member of the Growth-Associated Protein family that includes GAP-43 and MARCKS (24). BASP1 was initially found to be abundantly expressed in the central nervous system (25). BASP1 regulates nerve injury response and regeneration in part through modulating actin dynamics and presynaptic vesicle cycling. However, the regulation of BASP1 expression and its biological role in immune cells has not been explored. In this study, we found that BASP1 expression is highly enriched in myeloid cells in the liver and is markedly induced during diet-induced NASH. Conditional inactivation of BASP1 in myeloid cells ameliorates diet-induced NASH pathogenesis via attenuating pro-inflammatory signaling and hepatocyte injury.

Methods

Animal studies

All animal studies were performed using procedures approved by the Institutional Animal Care & Use Committee at the University of Michigan. Mice were housed in a selective pathogen-free facility under 12-hour light-dark cycles with free access to food and water. Mice were fed standard chow (Teklad 5001 Laboratory Diet), Choline-Deficient, Amino acid-defined (0.1% methionine) High-Fat (45% fat) Diet (CDA-HFD, A06071309, Research Diets Inc.), or NASH diet composed of 40% fat, 22% fructose, and 2% cholesterol (D09100301, Research Diets Inc.) to induce NASH, as described previously (21, 26).

To generate *floxed-Basp1* mouse strain, embryonic stem cells (C57BL/6N-A/a strain) bearing lox cassettes flanking exon 2 of *the Basp1* gene were obtained from the International Mouse Phenotype Consortium (mousephenotype.org/datagenes/MGI:1917600; Basp1tm2a(EUCOMM)Wtsi) and injected into blastocysts to generate chimeric mice. After identifying germline transmission, founder lines were crossed with C57BL/6 mice

expressing an FLP1 recombinase to eliminate the LacZ and neomycin-resistance cassettes. Myeloid-specific Basp1 knockout mice were generated by crossing Basp1 floxed mice with Lyz2-cre (LysMcre) mice.

Plasma assays

Plasma aspartate aminotransferase (AST) and alanine aminotransferase (ALT) levels were measured with commercial assay kits from Teco Diagnostics (A524–150) and Wako (995–34791), respectively. Plasma concentrations of cholesterol and triacyl glyceride (TAG) were measured using assay kits from Stanbio Laboratory (SB-1010–430) and Sigma (TR0100–1KT), respectively. Plasma CCL-2 (MCP-1) and TNFα concentrations were measured using Luminex 200 (R&D Systems).

Primary hepatocytes and liver macrophages culture

Primary hepatocytes were isolated from perfused wild-type C57BL/6J mouse liver following collagenase type II digestion. Hepatocytes were cultured in DMEM containing 10% bovine growth serum on collagen-coated plates. Liver NPCs were isolated as we previously described (21). Briefly, the livers were perfused and digested with pronase/collagenase. Liver cells were resuspended in DMEM containing 10% serum, centrifuged at 50g for 3 min to remove hepatocytes, and passed through a 40μm nylon cell strainer. This resulting cell suspension was subjected to density gradient centrifugation using 50% Optiprep (Axis Shield, 1114542) to remove cell debris. NPCs were collected and seeded into 6-well plates. Floating cells were removed after one hour and the remaining liver macrophages attached to the plates were cultured in DMEM containing 10% bovine growth serum.

BMDM culture

Bone marrow cells were isolated from the epiphyses of tibia and femur bones from young mice of 6 to 10 weeks of age. Red blood cells in cell suspension were lysed with 0.8% NH_4Cl for 3 minutes. After centrifugation at 250g for 5 minutes, cell pellets were resuspended in DMEM supplemented with 10% bovine growth serum, 100 μg/mL penicillin and streptomycin, and 25 ng/mL M-CSF (BioLegend, Cat:576406). After 6 days of culture, differentiated BMDMs were treated with vehicle or stimuli as indicated. For NLRP3 inflammasome activation, cultured BMDMs were primed with 200 ng/mL LPS (Sigma, Cat: L3012) for 2 or 4 hours followed by 3 mM ATP (Sigma, Cat: A3377) treatment for 30 minutes, as previously described (27). The concentrations of IL-1β in culture media were measured using Luminex 200 (R&D Systems).

Tissue histology and immunofluorescence staining

Liver tissues were fixed using formalin overnight and embedded in paraffin prior to sectioning. Hematoxylin and eosin (H&E) staining was used to assess steatosis and immune cell infiltration. Picrosirius (Sirius) Red (Polysciences, catalog 24901) staining was performed to evaluate liver fibrosis. For immunofluorescence staining, liver tissues were fixed with 4% paraformaldehyde (PFA) overnight, dehydrated in 30% sucrose in PBS overnight, and then embedded in optimal cutting temperature compound (OCT). Frozen sections were washed in PBS, permeabilized with 0.3% Triton X-100, and subsequently

blocked in 10% horse serum. Primary antibodies against MHC-II (1:200, 14–532185, Invitrogen), F4/80 (1:200, MCA497G, Bio-RAD), Decorin (1:200, AF-1060, R&D), and BASP1 (1:50, HPA045218, ATLAS ANTIBODIES) were incubated at 4°C overnight, followed by Alexa Fluor-conjugated secondary antibody (1:300, Invitrogen) at room temperature for 1 hour. Sections were stained with DAPI (Invitrogen, 10236276001) for 2 minutes after washing with PBS, mounted with VECTASHIELD Antifade Mounting Medium (Vector Laboratories, H-100), and imaged with fluorescence microscope.

Gene expression analysis

Total RNA was extracted using Trizol (Alkali Scientific, TRZ-100) method from frozen mouse livers and harvested cultured cells. Equal quantities of RNA were used to generate reverse-transcribed cDNA using the MMLV-RT method. Quantitative polymerase chain reaction (qPCR) using SYBR Green (Life Technologies) method was conducted for gene expression analysis. A list of qPCR primers is shown in Table S5.

Western Blot analysis

Liver samples were homogenized in a protein lysis buffer composed of 20 mM Tris (pH 7.5), 150 mM NaCl, 1 mM EDTA, 1 mM EGTA, 1% Triton X-100, and freshly added protease inhibitors (Roche) to prepare total protein lysates. BMDMs were harvested in lysis buffer containing 2% sodium dodecyl sulfate (SDS), 50 mM Tris-HCl (pH 6.8), 10 mM dithiothreitol (DTT), 10% glycerol, 0.002% bromophenol blue, and freshly added protease inhibitors. All protein lysates were boiled for 15 minutes, separated by SDS-PAGE, and then transferred to PVDF membrane. Antibodies against IL-1β, cleaved IL-1β, Caspase1, cleaved Caspase1, NLRP3 contained in a mouse reactive inflammasome antibody sampler kit (catalog 20836), and phosphorylation of NF-κB p65 (catalog 3033), SAPK/JNK (catalog 4668) were purchased from Cell Signaling Technology. Antibodies against HSP90 (Sc-13119), β-Actin (Sc-8432) and α-Tubulin (Sc-32293) were purchased from Santa Cruz. Trem2 antibody was a generous gift from Dr. Regina Feederle from the Monoclonal Antibody Core Facility of Helmholtz Zentrum Munchen. The ECL system used was BrightStar™ Duration HRP Chemiluminescent 2-Component Substrate ECL Kit (Alkali Scientific Inc, Cat: XR92).

Data analysis

Published RNA sequencing datasets were downloaded from Gene Expression Omnibus (GEO) database: single-cell RNAseq of mouse livers from chow and NASH diet-fed mice (GSE129516) (9); bulk RNAseq of mouse livers from chow and NASH diet-fed mice (GSE119340) (28); and bulk RNAseq of mouse livers from chow and CDA-HFD-fed mice (GSE120977) (29). scRNAseq dataset was processed and analyzed, as previously described (9, 21). DESeq2 was used for raw counts normalization and differentially expressed genes identification for bulk RNAseq (30). Gene ontology analysis was conducted using web-based resource (https://david.ncifcrf.gov/home.jsp). Feature plots, heatmaps, bubble plots, and violin plots were generated by R. GraphPad Prism was used to generate bar plots and scatter dot plots.

Statistical analysis

Statistical analyses were performed using GraphPad Prism 9. Student's t-test p value was calculated to evaluate the differences between two groups. One-way ANOVA followed by post hoc Tukey's test was used to determine the differences among multiple groups. Simple Linear Regression was performed for the correlation analysis.

Results

Reprogramming of the liver myeloid compartment in diet-induced NASH

Non-parenchymal cells (NPCs), including endothelial cells, hepatic stellate cells (HSCs), cholangiocytes, and diverse immune cell types, play a prominent role in liver tissue homeostasis and disease progression. We previously performed single-cell RNA sequencing analyses on NPCs isolated from healthy and diet-induced NASH mouse livers (9). Uniform Manifold Approximation and Projection (UMAP) analysis identified 11 clusters that represent major cell types in the liver, including 3,401 Kupffer cells (KCs), 4,221 monocyte-derived macrophages (MDMs), and 1,909 dendritic cells (DCs), collectively termed KDM cells (Figure 1A). Compared to chow-fed control, liver macrophages and DCs exhibited an approximately 3-fold expansion following diet-induced NASH. Despite this, the nature of NASH-associated myeloid cell reprogramming and its contribution to disease progression remain incompletely defined.

KCs are the resident liver macrophages originated from yolk sac during development, whereas MDMs represent macrophages matured from monocytes infiltrating the liver during NASH (14, 15). A subset of MDMs acquires the molecular signature and functional properties of KCs following the depletion of resident macrophages during chronic liver disease (20). To delineate the molecular nature of myeloid cell reprogramming in NASH, we first analyzed the transcriptomic signature of liver macrophage and DC populations. Analysis of the liver cell scRNAseq dataset revealed a total of 608 genes exhibiting enriched expression in the KDM cell clusters (Figure 1B; Table S1), including marker genes for KCs (Timd4, Clec4f, Vsig4), MDMs (Cx3cr1, Trem2, Gpnmb), and DCs (Siglech, Ccr9, Flt3). A subset of genes exhibited enriched expression in all three cell populations, such as H2-Ab1, a gene involved in the MHC class II-mediated antigen presentation pathway.

We next performed differential gene expression analysis to determine the extent to which these KDM-enriched genes are dysregulated during diet-induced NASH. Previous studies have demonstrated that mice fed a high-fructose, high-fat diet containing 2% dietary cholesterol (NASH diet) developed key features of NASH, including hepatocyte injury, inflammation, and liver fibrosis (26, 31). RNAseq analysis revealed a total of 234 differentially expressed KDM-enriched genes, 224 of which showed increased expression in the liver upon diet-induced NASH (Figure 1C; Table S2–S3). Similar transcriptomic changes were observed in another dietary NASH model using a choline-deficient, L-amino acid-defined, high-fat diet (CDA-HFD) (29). Analysis of bulk liver RNAseq dataset (GSE120977) from mice fed chow or CDA-HFD for 12 weeks revealed a total of 270 KDM-enriched genes exhibiting greater than 2-fold changes, 264 of which exhibited increased mRNA expression in the livers from mice fed CDA-HFD.

Among all differentially expressed KDM-enriched genes, 180 genes showed consistent alterations in both diet-induced NASH models, illustrating a common pattern of myeloid gene dysregulations in NASH liver (Figure 1D). Gene Ontology analysis indicated that differentially expressed myeloid genes are enriched for immune response, inflammatory response, antigen presentation, phagocytosis, and immune cell activation (Figure 1E). Expression of several KC marker genes, including Timd4, Clec4f, and Marco, was notably reduced in NASH liver, consistent with the depletion of resident macrophages during disease progression. These findings are consistent with a depletion of the resident macrophage population and a corresponding expansion of MDMs during chronic liver disease.

Induction of myeloid Basp1 expression in NASH liver

The increased expression of myeloid-enriched genes in NASH liver likely reflects a combination of myeloid cell expansion and altered gene expression in individual cells. Analysis of the sc-RNAseq dataset revealed that, compared to control, mRNA expression of 91 KDM-enriched genes was altered by more than 2-fold in cells isolated from NASH liver (Figure 2A; Table S4). Notably, mRNA expression of several KC-enriched genes (Cd163, Timd4, Fcna) was markedly downregulated at the single-cell level upon diet-induced NASH. In contrast, both KC and MDM clusters exhibited strongly increased expression of genes characteristic of NASH-associated macrophages NAMs (Trem2, Gpnmb), a unique population of monocyte-derived liver macrophages that emerged in mouse and human NASH (9). Interestingly, Brain abundant membrane attached signal protein 1 (BASP1), which is known to be abundantly expressed in the central nervous system and regulate nervous system development, exhibited high levels of expression in myeloid cells and was strongly induced following diet-induced NASH (Figure 2B and 1C). While Basp1 mRNA levels remained comparable in KCs isolated from healthy and NASH mouse livers, its expression was upregulated in the MDM and DC populations in NASH liver (Figure 2B and 2C). To explore the upstream signals that regulate Basp1 induction during NASH, we performed *in vitro* treatment on cultured bone marrow-derived macrophages (BMDMs). Our results indicated that, the combination of IL4 and IL10, but not pro-inflammatory stimuli (LPS+IFNγ) decreased Basp1 mRNA expression. In contrast, TGFβ robustly increased Basp1 expression in cultured macrophages (Figure 2D). Given that TGFβ expression is elevated in NASH liver, it is likely that TGFβ signaling contributes to the induction of Basp1 during NASH.

Accordingly, qPCR analysis confirmed that hepatic mRNA expression of Basp1 was increased by approximately 5 to 10-fold in two models of diet-induced NASH (Figure 3A). Immunofluorescence staining of liver sections from chow and NASH diet-fed mice revealed a marked increase of BASP1-positive cells in NASH liver (Figure 3B). Similar induction of BASP1 mRNA expression was observed in human liver biopsies from individuals with NASH compared to non-NASH control (Figure 3C). These findings illustrate that Basp1 induction is likely a conserved feature of myeloid reprogramming during NASH progression. We previously demonstrated that a NASH to chow dietary switch resulted in the resolution of key NASH features (28). To investigate whether hepatic Basp1 expression is responsive to NASH resolution, we examined its mRNA levels in mice fed NASH diet and two separate cohorts following NASH to chow dietary switch for 1 or 2 months. As shown

in Figure 3D, NASH-associated induction of Basp1 expression was significantly decreased in the liver following the dietary switch in a time-dependent manner.

To determine whether hepatic Basp1 expression correlates with NASH severity, we examined its mRNA levels in a cohort of NASH diet-fed mice that exhibited different degree of liver injury. Basp1 mRNA expression in the liver was strongly associated with plasma AST and ALT levels (Figure 4A). In addition, Basp1 mRNA levels strongly correlated with mRNA expression of Col1a1, Adgre1, Ccl2, and H2-Ab1, genes associated with liver fibrosis and inflammatory response. To determine whether Basp1 induction occurs in early stages of NAFLD, we examined its expression in a cohort of high-fat diet-fed mice that exhibited a different degree of weight gain and hepatic steatosis. Interestingly, hepatic Basp1 mRNA levels displayed a strong association with the severity of obesity (body weight), liver fat content, and Col1a1 mRNA levels (Figure 4B). Together, these results demonstrate that increased hepatic Basp1 levels are a conserved feature of human and mouse NASH and a molecular marker associated with NASH severity.

Myeloid-specific inactivation of Basp1 protects mice from diet-induced NASH

Previous studies have established Basp1 as a versatile regulator of actin cytoskeleton, gene transcription, synaptic function, and neurodevelopment (24). However, the biological role of Basp1 in inflammatory signaling and NASH pathogenesis have not been explored. It is possible that increased Basp1 levels may alter the balance of pro- and anti-inflammatory signaling in myeloid cells, thereby contributing to disease progression. To test this, we generated mice with myeloid-specific inactivation of Basp1 (MKO) by crossing Basp1-floxed mice with Lyz2-cre (LysMcre) mice. We subjected three-month old male control (flox/flox) and MKO littermates to NASH diet feeding for 20 weeks (Figure 5A). MKO mice gained slightly more weight with higher liver to body weight ratio than control following NASH diet feeding (Figure 5B). Measurements of liver injury markers indicated that plasma ALT and AST levels were significantly lower in MKO mice than control (Figure 5C), suggesting that myeloid-specific ablation of Basp1 ameliorated NASH-associated hepatocyte injury. MKO mice exhibited slightly higher blood glucose and plasma triglyceride (TAG) and cholesterol concentrations (Figure 5D). While total liver fat content remained comparable between two groups, histological staining revealed that hepatocytes from MKO mice contained abundant smaller lipid droplets and fewer large lipid droplets (Figure 5D–5E). These results demonstrate that myeloid inactivation of Basp1 improves diet-induced NASH pathologies in mice and may modulate hepatic lipid metabolism via non-cell autonomous mechanisms.

Consistent with improved liver injury, MKO mice exhibited less pronounced liver fibrosis as indicated by Sirius Red staining (Figure 6A). Compared to control, pericellular collagen deposition was greatly reduced in Basp1 MKO mouse livers. Immunofluorescence staining of Decorin, a protein highly expressed by HSC during liver fibrosis, showed a concordant decrease in Basp1 conditional null mice (Figure 6B). Hepatic gene expression analysis indicated that mRNA expression of fibrosis-related genes (Col1a1, Col1a2, Tgfb) was diminished in MKO livers, whereas mRNA levels of Acta2, a marker for HSC activation, remained comparable between two groups (Figure 6C). While the

expression of genes involved in hepatic lipid metabolism remained similar, mRNA level of Fsp27, which encodes a lipid droplet protein, was significantly reduced in MKO mouse livers. Additionally, mRNA expression of several genes involved in bile acid synthesis (Cyp7a1, Cyp7b1, Cyp8b1, Cyp27a1) and transport (Baat, Abcb11, Slc10a1, Slc10a2) were significantly increased in Basp1 MKO mouse livers. These findings suggest that myeloid Basp1 may influence hepatic cholesterol and bile acid metabolism, likely through a non-cell autonomous mechanism. Interestingly, mRNA expression of several genes associated with regulatory T cells (Foxp3) and CD8+ T cell exhaustion (Tox, Pdcd1), hallmarks of NASH-associated remodeling of the liver immune microenvironment, was also attenuated upon inactivation of Basp1 in myeloid cells (Figure 6C). We did not observe significant differences between control and MKO mice under chow-fed conditions (Figure S1), suggesting that myeloid Basp1 is uniquely important during liver injury and disease progression.

Basp1 deficiency attenuates proinflammatory signaling in macrophages

Myeloid cells play an integral role within the liver microenvironment through recognizing and phagocytosing dead cells, presenting antigens to the immune system, and releasing cytokines that initiate and/or propagate immune responses during liver injury. We next examined the role of Basp1 in the regulation of NASH-associated liver inflammation. Compared to control, plasma CCL2 and TNFα levels were significantly lower in MKO mice (Figure 7A). Consistently, qPCR analysis indicated that hepatic mRNA expression of proinflammatory cytokines (Tnf, Ccl2) and NLRP3 inflammasome-related genes (Nlrp3, Pycard, Il1b) was significantly attenuated by Basp1 inactivation (Figure 7B). Immunofluorescence staining of liver sections revealed that the abundance of F4/80-positive macrophages was reduced by Basp1 inactivation (Figure 7C). Similarly, the abundance of antigen-presenting cells expressing H2-AB1, a subunit of the MHC II antigen presentation complex, was greatly reduced in the Basp1 MKO mouse liver. We previously identified a unique population termed NAMs that express marker genes, including Trem2, Gpnmb, and Mmp12 (9). Interestingly, Basp1 deficiency resulted in slightly elevated NAM marker gene expression at both mRNA and protein levels in MKO NASH livers, without increasing other macrophage/myeloid cell markers (Adgre1, Marco, Ccr2) (Figure 7D–7E).

To determine whether Basp1 deficiency directly impacts inflammatory signaling in macrophages, we cultured bone marrow-derived macrophages (BMDMs) isolated from control and Basp1 MKO mice and performed treatments with LPS plus Interferon γ (IFNγ). As expected, LPS in combination with IFNγ potently stimulated mRNA expression of proinflammatory cytokines, such as Tnf, Ccl2, and Il12b, after 24 hours of treatment. This cytokine response was significantly impaired in Basp1-deficient macrophages (Figure 8A). We conducted similar experiments using primary liver macrophages isolated from NASH diet-fed control and MKO mice. qPCR analysis indicated that the induction of proinflammatory cytokines (Tnf, Il12b, and Il1b) in response to LPS was greatly diminished in Basp1-deficient liver macrophages (Figure 8B). Accordingly, activation of proinflammatory signaling pathways, including NF-κB and SAPK/JNK pathways, was diminished in the absence of Basp1 (Figure S2A). Recent studies have demonstrated that NLRP3 inflammasome activation promotes NASH progression in mice (17). We

next examined whether Basp1 plays a role in NLRP3 inflammasome activation following stimulation by LPS plus ATP. Compared to control, protein levels of cleaved Caspase-1 and IL-1β, molecular markers of NLRP3 inflammasome activation, were strongly attenuated in Basp1-deficient BMDMs and liver macrophages (Figure 8C–8D). Additionally, the concentrations of IL-1β in conditioned media from MKO BMDMs were significantly lower than control (Figure S2B). To determine whether myeloid Basp1 signaling may contribute to hepatocyte injury, we incubated primary hepatocytes with conditioned media from BMDMs and assayed hepatocyte death using flow cytometry. Compared to unstimulated control, NLRP3 activation strongly increased hepatocyte death (Figure S2C). Basp1 inactivation slightly but significantly attenuated cytotoxic effects of BMDM media on hepatocytes. Together, our findings demonstrated that Basp1 ablation blunted proinflammatory signaling and NLRP3 inflammasome activation in macrophages.

Discussion

Innate immunity serves to defend the body against pathogens and contributes to tissue homeostasis and disease progression. The immune cells of myeloid origin, particularly monocyte-derived macrophages and dendritic cells, play an important role in shaping the liver microenvironment during NASH (14, 15). Recent single-cell transcriptomic studies have provided new insights into the nature of macrophage heterogeneity and reprogramming in the context of liver injury and fibrotic response. The marked infiltration and expansion of monocyte-derived macrophages are characteristics of NASH liver. In addition to its increased abundance, a subpopulation of MDMs acquire a unique molecular signature characterized by the expression of marker genes, such as Trem2 and Gpnmb (7, 9, 20). These NASH-associated macrophages contribute to forming a fibrotic niche in the liver (32). In parallel, an increased abundance of conventional dendritic cells has been observed in human and mouse NASH, which display a more activated molecular signature (33, 34). Despite the critical role of these myeloid-derived cells in liver injury response and disease progression, the mechanisms that balance pro-inflammatory and anti-inflammatory signaling by innate immune cells in NASH liver remain incompletely understood. In this study, we analyzed the transcriptomic landscape of liver resident macrophages, MDMs, and dendritic cells, and uncovered Basp1 as an important factor that contributes to diet-induced NASH by facilitating pro-inflammatory signaling and NLRP3 inflammasome activation.

A notable feature of NASH liver transcriptome is the marked induction of gene signatures characteristic of KC, MDM, and DC lineages. Elevated expression of genes involved in innate immune response, phagocytosis and antigen presentation likely reflects a combination of increased infiltration of immune cells into the liver and reprogramming of gene expression in individual cell types. Compared to healthy liver, the relative abundance of KDM cells increased by approximately 3-fold in the liver upon diet-induced NASH. Analysis of single-cell RNAseq data revealed that a subset of KCs and MDMs share a unique transcriptomic signature featured by the expression of a set of marker genes, including Trem2, Gpnmb, Mmp12, and Basp1 (Figure 2A). Basp1 exhibits a broader expression profile than Trem2; its mRNA is detectable in all macrophage subtypes and dendritic cells. Basp1 mRNA expression is strongly increased in two dietary models of NASH in mice and in human NASH livers. Importantly, hepatic Basp1 levels return to lower

levels upon NASH resolution following NASH to chow dietary switch in mice, suggesting that Basp1 may play a role in modulating NASH progression and resolution. Previous studies have established that BASP1 is regulated at transcriptional and post-translational levels via myristoylation, phosphorylation, and phase separation (24, 25, 35). It is likely that these post-translational modifications may provide additional mechanisms to regulate the biological functions of Basp1 in innate immune cells.

We found that myeloid-specific ablation of Basp1 attenuates the severity of NASH pathologies in mice. Because Basp1 inactivation using LysM-cre occurs in all bone marrow-originated myeloid cells, the relative importance of MDMs and DCs in mediating the protective effects of Basp1 ablation on NASH remains to be clarified. At the mechanistic level, Basp1 deficiency impairs pro-inflammatory signaling in cultured BMDMs, notably activation of the NLRP3 inflammasome. Previous studies have implicated excess NLRP3 inflammasome activation as a pathogenic driver of NASH progression (17). Genetic or pharmacological blockade of NLRP3 activation exerts robust protective effects on diet-induced NASH (16, 18, 19, 36). The exact molecular mechanisms that link BASP1 to inflammasome activation and its role in mediating the effects of Basp1 inactivation on NASH remain currently unknown. As Basp1 exerts diverse effects on cellular signaling and function, we cannot rule out potential contributions from NLRP3-independent mechanisms in mediating its effects on NASH. An intriguing observation from the current study is that ablation of Basp1 in myeloid cells results in smaller lipid droplets in hepatocytes without altering liver fat content. It is possible that cytokines and/or extracellular vesicles released by macrophages and dendritic cells may elicit these metabolic effects in hepatocytes.

Supplementary Material

Refer to Web version on PubMed Central for supplementary material.

Acknowledgements

We thank Dr. Regina Feederle at the Monoclonal Antibody Core Facility of Helmholtz Zentrum Munchen, Germany for sharing the Trem2 antibody, and Xiaoling Peng for providing technical support. We thank the University of Michigan Transgenic Animal Model Core for the generation of Basp1 knockout mice. This work was supported by NIH (DK136179 to J.D.L. and DK124709 to K.I.). L.Z. was supported by the American Heart Association Career Development Award. Graphical abstract was created with BioRender.com.

References

1. Sheka AC, Adeyi O, Thompson J, Hameed B, Crawford PA, Ikramuddin S. Nonalcoholic Steatohepatitis: A Review. JAMA 2020;323:1175–1183. [PubMed: 32207804]
2. Bence KK, Birnbaum MJ. Metabolic drivers of non-alcoholic fatty liver disease. Mol Metab 2021;50:101143. [PubMed: 33346069]
3. Loomba R, Friedman SL, Shulman GI. Mechanisms and disease consequences of nonalcoholic fatty liver disease. Cell 2021;184:2537–2564. [PubMed: 33989548]
4. Schwabe RF, Tabas I, Pajvani UB. Mechanisms of Fibrosis Development in Nonalcoholic Steatohepatitis. Gastroenterology 2020;158:1913–1928. [PubMed: 32044315]
5. Rui L, Lin JD. Reprogramming of Hepatic Metabolism and Microenvironment in Nonalcoholic Steatohepatitis. Annu Rev Nutr 2022.
6. Rosenthal SB, Liu X, Ganguly S, Dhar D, Pasillas MP, Ricciardelli E, Li RZ, et al. Heterogeneity of HSCs in a Mouse Model of NASH. Hepatology 2021;74:667–685. [PubMed: 33550587]

7. Seidman JS, Troutman TD, Sakai M, Gola A, Spann NJ, Bennett H, Bruni CM, et al. Niche-Specific Reprogramming of Epigenetic Landscapes Drives Myeloid Cell Diversity in Nonalcoholic Steatohepatitis. Immunity 2020;52:1057–1074 e1057. [PubMed: 32362324]
8. Wang S, Li K, Pickholz E, Dobie R, Matchett KP, Henderson NC, Carrico C, et al. An autocrine signaling circuit in hepatic stellate cells underlies advanced fibrosis in nonalcoholic steatohepatitis. Sci Transl Med 2023;15:eadd3949.
9. Xiong X, Kuang H, Ansari S, Liu T, Gong J, Wang S, Zhao XY, et al. Landscape of Intercellular Crosstalk in Healthy and NASH Liver Revealed by Single-Cell Secretome Gene Analysis. Mol Cell 2019;75:644–660 e645. [PubMed: 31398325]
10. Xiao Y, Batmanov K, Hu W, Zhu K, Tom AY, Guan D, Jiang C, et al. Hepatocytes demarcated by EphB2 contribute to the progression of nonalcoholic steatohepatitis. Sci Transl Med 2023;15:eadc9653.
11. Xiong J, Liu T, Mi L, Kuang H, Xiong X, Chen Z, Li S, et al. hnRNPU/TrkB Defines a Chromatin Accessibility Checkpoint for Liver Injury and Nonalcoholic Steatohepatitis Pathogenesis. Hepatology 2020;71:1228–1246. [PubMed: 31469911]
12. Hammoutene A, Rautou PE. Role of liver sinusoidal endothelial cells in non-alcoholic fatty liver disease. J Hepatol 2019;70:1278–1291. [PubMed: 30797053]
13. Terkelsen MK, Bendixen SM, Hansen D, Scott EAH, Moeller AF, Nielsen R, Mandrup S, et al. Transcriptional Dynamics of Hepatic Sinusoid-Associated Cells After Liver Injury. Hepatology 2020;72:2119–2133. [PubMed: 32145072]
14. Guilliams M, Scott CL. Liver macrophages in health and disease. Immunity 2022;55:1515–1529. [PubMed: 36103850]
15. Peiseler M, Schwabe R, Hampe J, Kubes P, Heikenwalder M, Tacke F. Immune mechanisms linking metabolic injury to inflammation and fibrosis in fatty liver disease - novel insights into cellular communication circuits. J Hepatol 2022;77:1136–1160. [PubMed: 35750137]
16. Kaufmann B, Kui L, Reca A, Leszczynska A, Kim AD, Booshehri LM, Wree A, et al. Cell-specific Deletion of NLRP3 Inflammasome Identifies Myeloid Cells as Key Drivers of Liver Inflammation and Fibrosis in Murine Steatohepatitis. Cell Mol Gastroenterol Hepatol 2022;14:751–767. [PubMed: 35787975]
17. Knorr J, Wree A, Tacke F, Feldstein AE. The NLRP3 Inflammasome in Alcoholic and Nonalcoholic Steatohepatitis. Semin Liver Dis 2020;40:298–306. [PubMed: 32526788]
18. Mridha AR, Wree A, Robertson AAB, Yeh MM, Johnson CD, Van Rooyen DM, Haczeyni F, et al. NLRP3 inflammasome blockade reduces liver inflammation and fibrosis in experimental NASH in mice. J Hepatol 2017;66:1037–1046. [PubMed: 28167322]
19. Wree A, McGeough MD, Pena CA, Schlattjan M, Li H, Inzaugarat ME, Messer K, et al. NLRP3 inflammasome activation is required for fibrosis development in NAFLD. J Mol Med (Berl) 2014;92:1069–1082. [PubMed: 24861026]
20. Daemen S, Gainullina A, Kalugotla G, He L, Chan MM, Beals JW, Liss KH, et al. Dynamic Shifts in the Composition of Resident and Recruited Macrophages Influence Tissue Remodeling in NASH. Cell Rep 2022;41:111660. [PubMed: 36384118]
21. Zhang P, Chen Z, Kuang H, Liu T, Zhu J, Zhou L, Wang Q, et al. Neuregulin 4 suppresses NASH-HCC development by restraining tumor-prone liver microenvironment. Cell Metab 2022;34:1359–1376 e1357. [PubMed: 35973424]
22. Hou J, Zhang J, Cui P, Zhou Y, Liu C, Wu X, Ji Y, et al. TREM2 sustains macrophage-hepatocyte metabolic coordination in nonalcoholic fatty liver disease and sepsis. J Clin Invest 2021;131.
23. Wang X, He Q, Zhou C, Xu Y, Liu D, Fujiwara N, Kubota N, et al. Prolonged hypernutrition impairs TREM2-dependent efferocytosis to license chronic liver inflammation and NASH development. Immunity 2023;56:58–77 e11. [PubMed: 36521495]
24. Chung D, Shum A, Caraveo G. GAP-43 and BASP1 in Axon Regeneration: Implications for the Treatment of Neurodegenerative Diseases. Front Cell Dev Biol 2020;8:567537. [PubMed: 33015061]
25. Mosevitsky MI, Capony JP, Skladchikova G, Novitskaya VA, Plekhanov A, Zakharov VV. The BASP1 family of myristoylated proteins abundant in axonal termini. Primary structure analysis and physico-chemical properties. Biochimie 1997;79:373–384. [PubMed: 9310187]

26. Guo L, Zhang P, Chen Z, Xia H, Li S, Zhang Y, Kobberup S, et al. Hepatic neuregulin 4 signaling defines an endocrine checkpoint for steatosis-to-NASH progression. J Clin Invest 2017;127:4449–4461. [PubMed: 29106384]
27. Youm YH, Nguyen KY, Grant RW, Goldberg EL, Bodogai M, Kim D, D'Agostino D, et al. The ketone metabolite beta-hydroxybutyrate blocks NLRP3 inflammasome-mediated inflammatory disease. Nat Med 2015;21:263–269. [PubMed: 25686106]
28. Xiong X, Wang Q, Wang S, Zhang J, Liu T, Guo L, Yu Y, et al. Mapping the molecular signatures of diet-induced NASH and its regulation by the hepatokine Tsukushi. Mol Metab 2019;20:128–137. [PubMed: 30595550]
29. Min-DeBartolo J, Schlerman F, Akare S, Wang J, McMahon J, Zhan Y, Syed J, et al. Thrombospondin-I is a critical modulator in non-alcoholic steatohepatitis (NASH). PLoS One 2019;14:e0226854. [PubMed: 31891606]
30. Love MI, Huber W, Anders S. Moderated estimation of fold change and dispersion for RNA-seq data with DESeq2. Genome Biol 2014;15:550. [PubMed: 25516281]
31. Clapper JR, Hendricks MD, Gu G, Wittmer C, Dolman CS, Herich J, Athanacio J, et al. Diet-induced mouse model of fatty liver disease and nonalcoholic steatohepatitis reflecting clinical disease progression and methods of assessment. Am J Physiol Gastrointest Liver Physiol 2013;305:G483–495. [PubMed: 23886860]
32. Ramachandran P, Dobie R, Wilson-Kanamori JR, Dora EF, Henderson BEP, Luu NT, Portman JR, et al. Resolving the fibrotic niche of human liver cirrhosis at single-cell level. Nature 2019;575:512–518. [PubMed: 31597160]
33. Deczkowska A, David E, Ramadori P, Pfister D, Safran M, Li B, Giladi A, et al. XCR1(+) type 1 conventional dendritic cells drive liver pathology in non-alcoholic steatohepatitis. Nat Med 2021;27:1043–1054. [PubMed: 34017133]
34. Haas JT, Vonghia L, Mogilenko DA, Verrijken A, Molendi-Coste O, Fleury S, Deprince A, et al. Transcriptional Network Analysis Implicates Altered Hepatic Immune Function in NASH development and resolution. Nat Metab 2019;1:604–614. [PubMed: 31701087]
35. Zakharov VV, Mosevitsky MI. Oligomeric structure of brain abundant proteins GAP-43 and BASP1. J Struct Biol 2010;170:470–483. [PubMed: 20109554]
36. Cai C, Zhu X, Li P, Li J, Gong J, Shen W, He K. NLRP3 Deletion Inhibits the Non-alcoholic Steatohepatitis Development and Inflammation in Kupffer Cells Induced by Palmitic Acid. Inflammation 2017;40:1875–1883. [PubMed: 28730512]

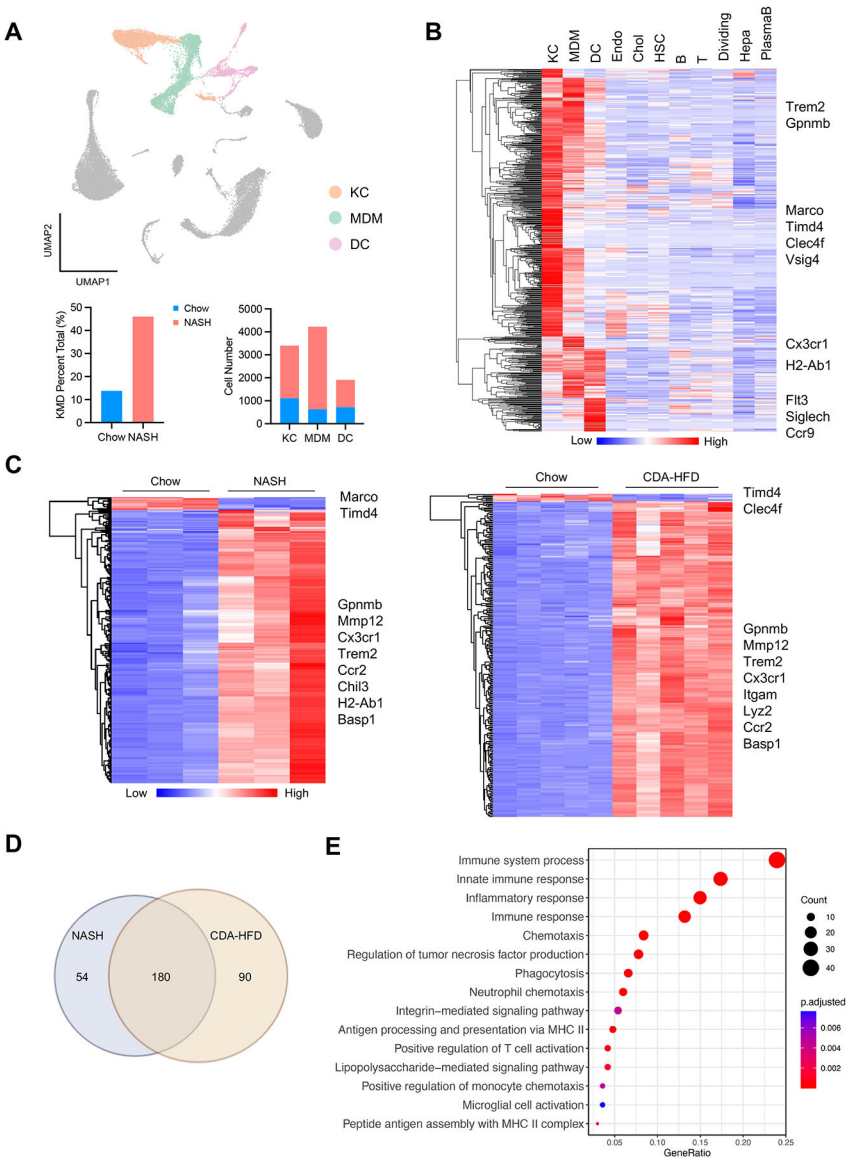

Figure 1. Transcriptomic signatures of the resident macrophage and recruited myeloid cell compartments in NASH liver.

A) UMAP visualization of liver cell clusters based on single-cell RNA sequencing analysis of liver non-parenchymal cells isolated from mice fed chow or NASH diet (GSE129516) (up). Bar plots of cell number and percentage of KDM cells in chow and NASH mouse livers (down).

B) Heatmap of genes exhibiting enriched expression in Kupffer cells (KC), Monocyte-derived macrophages (MDM), and Dendritic cells (DC) based on averaged expression levels in individual cell types. A total of 608 genes exhibited highest mRNA expression in one of the KDM cell types with average normalized Unique Molecular Identifiers (UMIs) > 1.

C) Heatmap of differentially expressed macrophage/myeloid-enriched genes based on bulk RNAseq data from mice fed with chow or NASH diet for 20 weeks (left, GSE119340), and chow or CDA-HFD for 12 weeks (right, GSE120977). 234 and 270 genes passed the filter

of adjusted P-value < 0.05 and Log2 Fold Change (NASH/chow) > 1 in two dietary NASH models, respectively.

D) Venn diagram of differentially expressed macrophage/myeloid-enriched genes in two NASH models.

E) Bubble plot of Gene Ontology analysis of differentially expressed macrophage/myeloid-enriched genes in NASH liver.

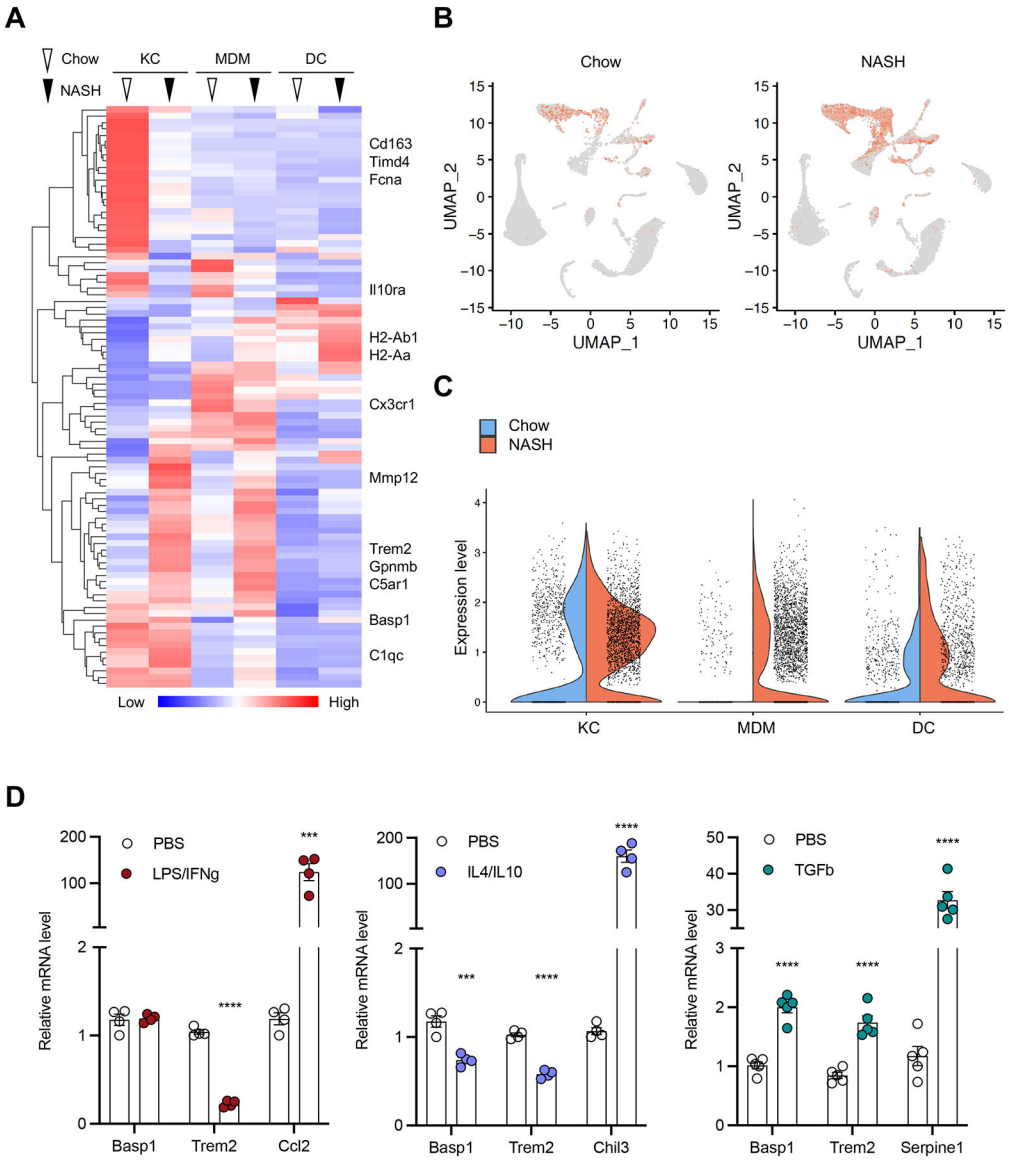

Figure 2. Regulation of Basp1 expression during NASH and in cultured macrophages.

A) Heatmap of differentially expressed genes in KDM cells based on sc-RNAseq data from mice fed with chow or NASH diet for 20 weeks. 91 genes passed the filter of average UMI > 1 and Log2 Fold Change (NASH/chow) > 1 in at least one of three cell types.

B) Feature plot illustrating mRNA expression of Basp1 in individual liver cells from mice fed chow or NASH diet.

C) Violin plot illustrating mRNA expression of Basp1 in KDM clusters.

D) qPCR analysis of gene expression in cultured BMDMs treated with PBS or LPS (5 ng/mL) plus IFN-γ (5 ng/mL), IL-4 (5 ng/mL) plus IL-10 (5 ng/mL), or TGF-β (2.5 ng/mL) for 24 hours, as indicated.

Data in D) represent mean ± SEM; ***p < 0.001, ****p < 0.0001. Two-tailed unpaired Student's *t*-test.

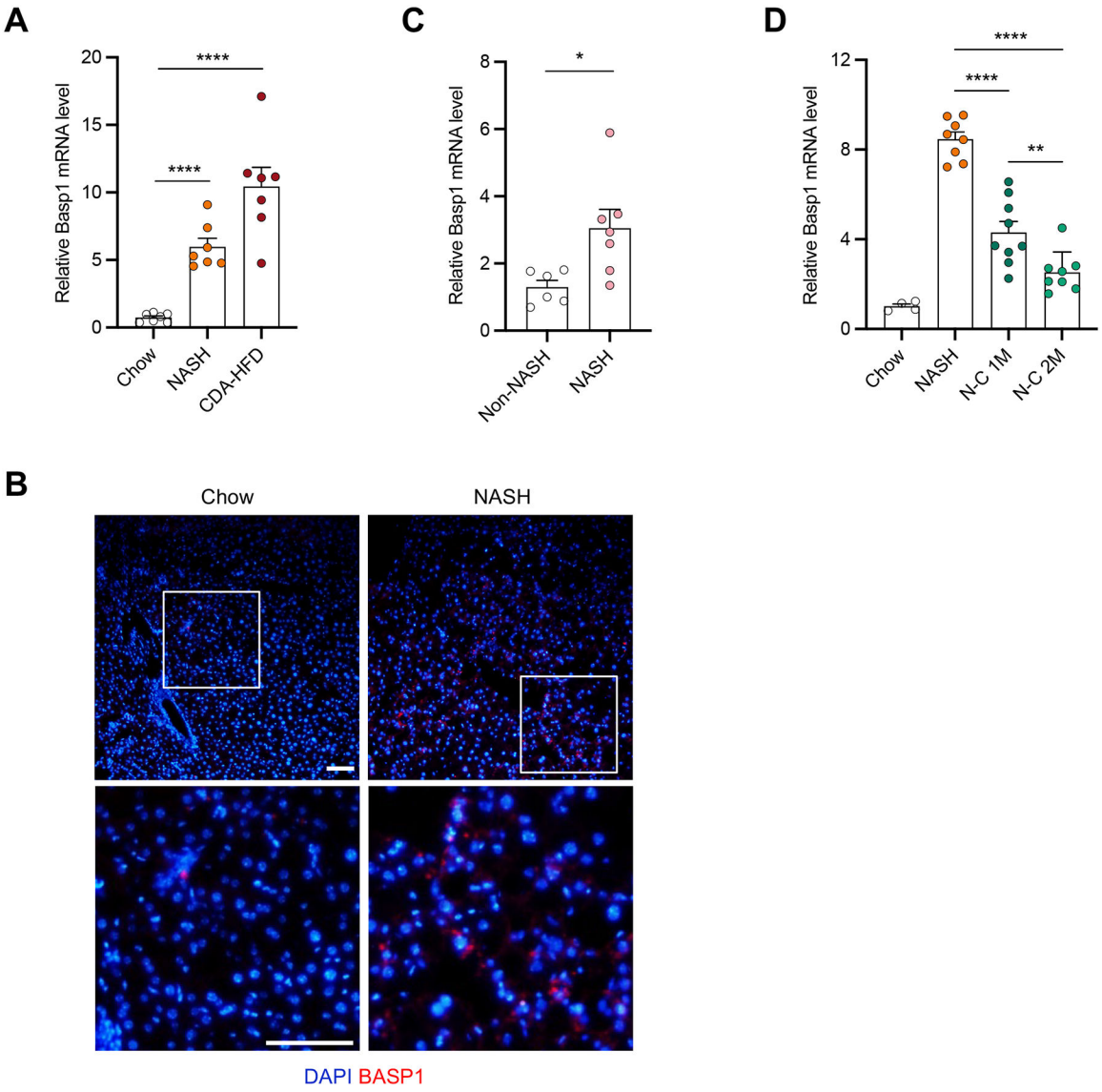

Figure 3. Regulation of BASP1 expression during NASH and NASH resolution.

A) qPCR analysis of hepatic Basp1 expression in mice fed chow (n = 7), NASH diet for 20 weeks (n = 7), or CDA-HFD for 8 weeks (n = 7). Age-matched mice were divided into three dietary cohorts and harvested at the same time following indicated feeding time.

B) BASP1 immunofluorescence staining of liver sections. Scale bars, 100μm.

C) qPCR analysis of human hepatic Basp1 expression in non-NASH (n = 6) or NASH patients (n = 7).

D) qPCR analysis of hepatic Basp1 expression in mice fed chow (n = 4), NASH diet for 6 months (n = 8), or 4 months NASH diet followed by switching to chow for 1 month (n = 9) or 2 months (n = 8).

Data in C) represent mean ± SEM; *$p < 0.05$, analyzed by two-tailed unpaired Student's *t*-test. Data in A) and D) represent mean ± SEM; **$p < 0.01$, ****$p < 0.0001$, analyzed by one-way ANOVA with post hoc analysis using Tukey's test.

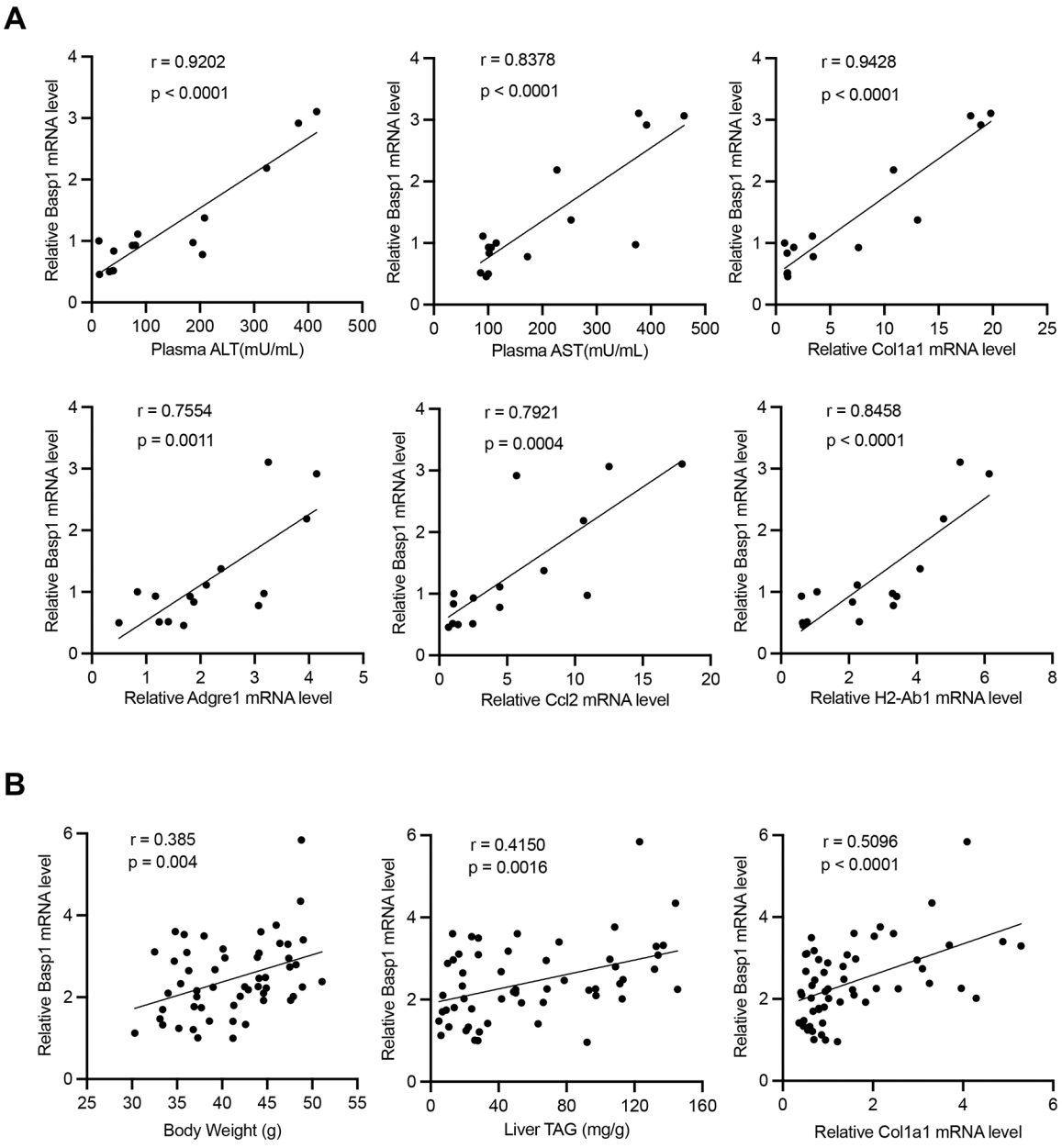

Figure 4. Correlation of Basp1 expression with metabolic liver disease.

A) Correlation of hepatic Basp1 mRNA level with plasma ALT and AST levels, and hepatic mRNA levels of Col1a1, Adgre1, Ccl2, and H2-Ab1 in mice fed NASH (n = 11) or chow (n = 4) diet for 12 weeks.

B) Correlation of hepatic Basp1 mRNA level with body weight, liver TAG content, and hepatic Col1a1 mRNA level in mice fed HFD for 8 weeks (n = 55).

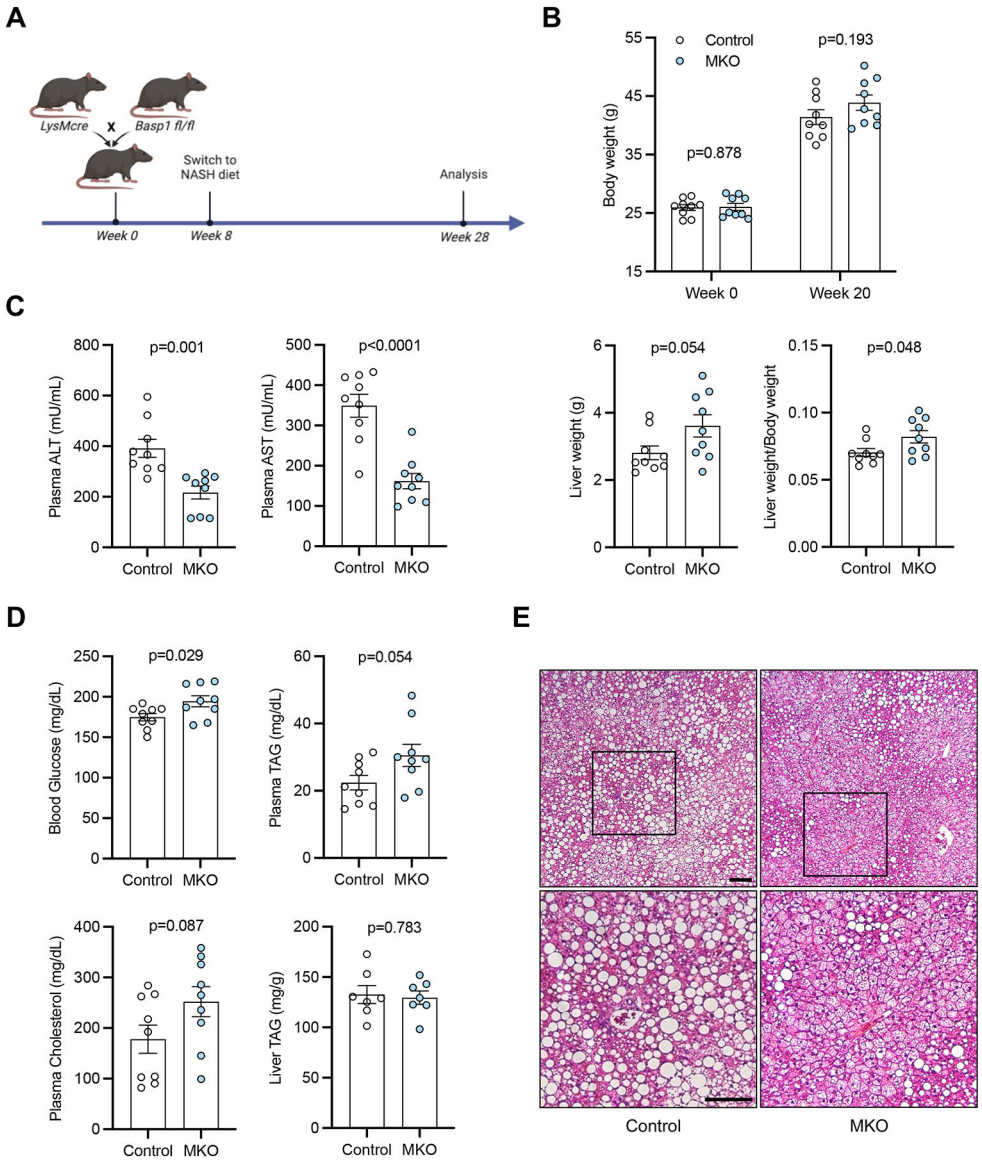

Figure 5. Myeloid-specific ablation of Basp1 ameliorates liver injury during NASH.

A) A schematic outline of the NASH liver study.

B) Body weight, liver weight, and liver/body weight ratio of control (n = 9) and MKO (n = 9) mice following 20 weeks of NASH diet feeding.

C) Plasma ALT and AST levels in control and MKO mice after 20 weeks of NASH diet feeding.

D) Metabolic parameters of NASH diet-fed mice.

E) H&E histology of liver sections from NASH diet-fed mice. Scale bars, 100 μm.

Data represent mean ± SEM. Two-tailed unpaired Student's *t*-test.

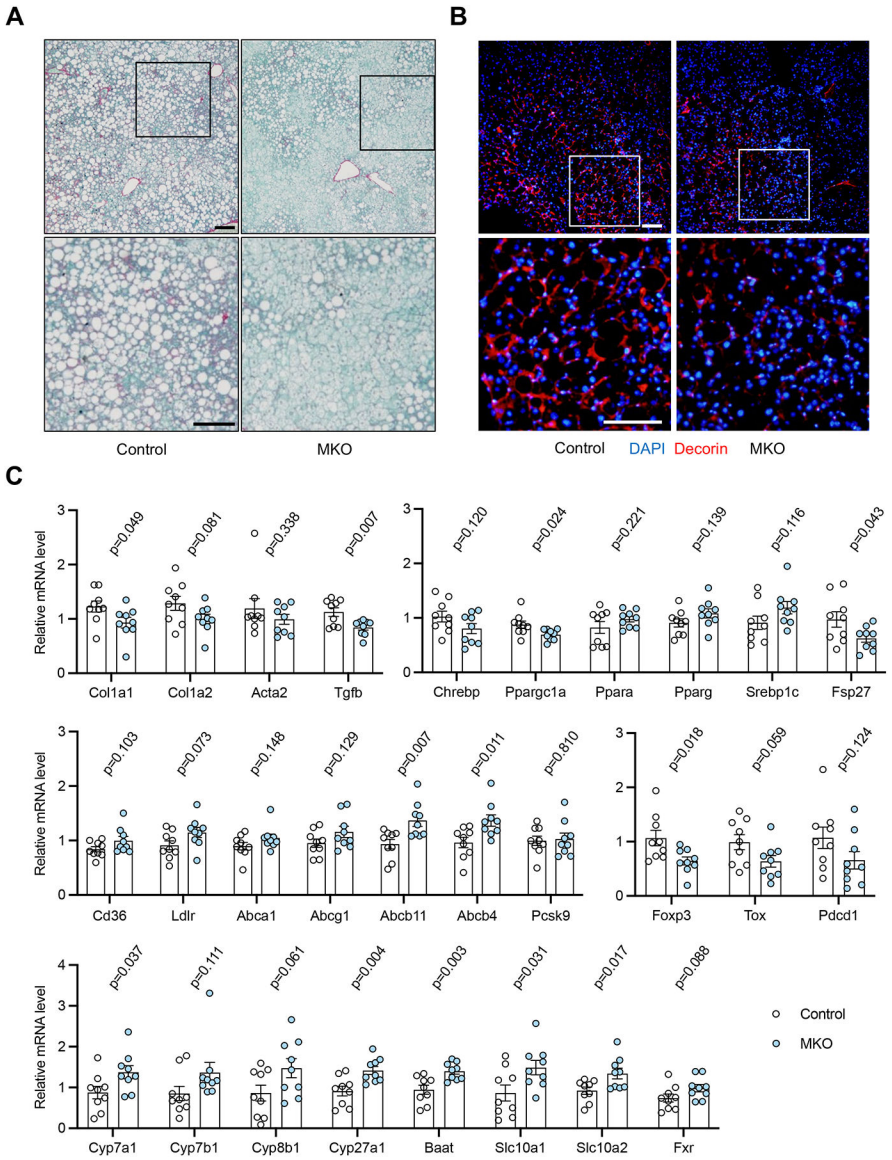

Figure 6. Basp1 ablation in myeloid cells improves diet-induced NASH pathologies in mice.

A) Sirius Red staining of liver sections from NASH diet-fed mice. Scale bars, 100 μm.

B) Decorin immunofluorescence staining. Scale bars, 100 μm.

C) qPCR analysis of hepatic gene expression from NASH diet-fed mice.

Data represent mean ± SEM. Two-tailed unpaired Student's *t*-test.

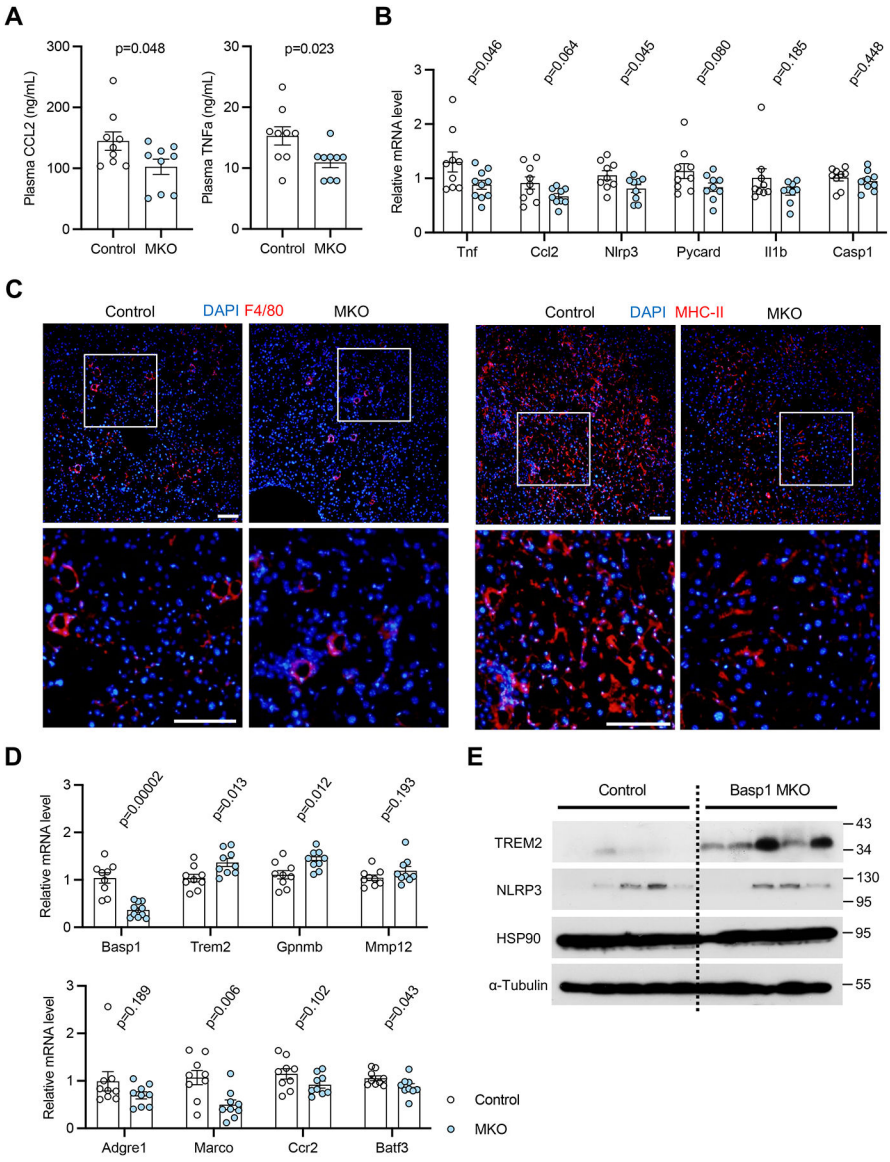

Figure 7. Effects of myeloid-specific Basp1 inactivation on liver inflammation.

A) Plasma CCL-2 and TNFα levels in control and MKO mice after 20 weeks of NASH diet feeding.

B) qPCR analysis of hepatic expression of inflammation- and NLRP3 inflammasome-related genes in NASH diet-fed mice.

C) F4/80 (left) and MHC-II (right) immunofluorescence staining. Scale bars, 100 μm.

D) qPCR analysis of hepatic gene expression in NASH diet-fed mice.

E) Immunoblots of liver lysates from NASH diet-fed mice.

Data represent mean ± SEM. Two-tailed unpaired Student's *t*-test.

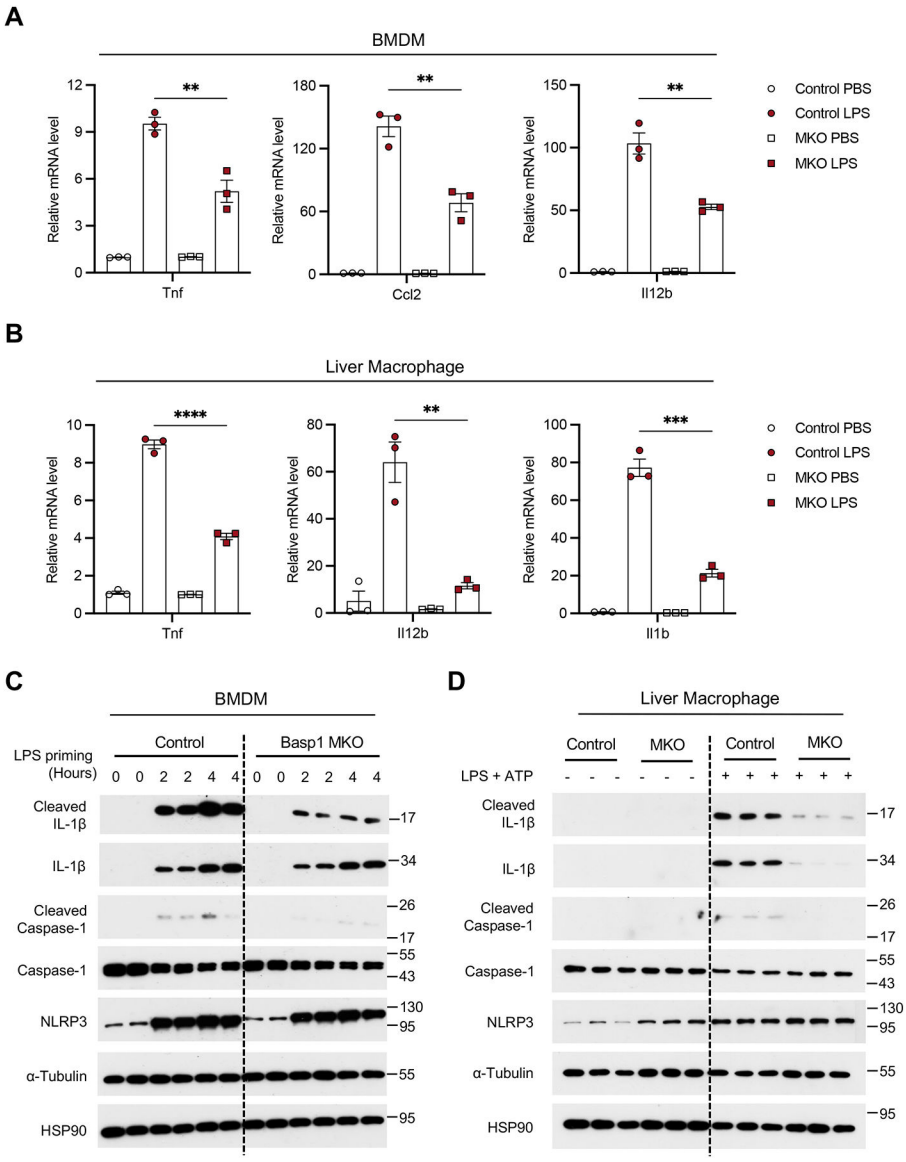

Figure 8. Basp1 inactivation attenuates proinflammatory signaling and NLRP3 inflammasome activation in cultured macrophages.

A) qPCR analysis of gene expression in cultured BMDMs treated with PBS or LPS (5 ng/mL) plus IFN-γ (5 ng/mL) for 24 hours.

B) qPCR analysis of gene expression in cultured liver macrophages isolated from NASH livers treated with PBS or LPS (5 ng/mL) plus IFN-γ (5 ng/mL) for 24 hours.

C) Immunoblots of total protein lysates from cultured BMDMs isolated from control and MKO mice. Differentiated macrophages were treated with PBS or LPS (200 ng/mL) for indicated time followed by ATP (3 mM) treatment for 30 minutes.

D) Immunoblots of total protein lysates from cultured liver macrophages isolated from NASH diet-fed control and MKO mice. Primary macrophages were treated with PBS or LPS (200 ng/mL) for 3 hours followed by ATP (3 mM) treatment for 30 minutes.

Data in A) and B) represent mean ± SEM; **p < 0.01, ***p < 0.001, ****p < 0.0001. Two-tailed unpaired Student's *t*-test.